energies

MDPI

Article

Mechanical and Optical Characterization of 0.7 mm Ion-Exchange-Strengthened Aluminosilicate Glass for Building-Integrated Photovoltaics

Paweł Kwaśnicki [1,2,3,*], Ludmiła Marszałek [2], Dariusz Augustowski [2], Anna Gronba-Chyła [3] and Agnieszka Generowicz [4,5,*]

[1] Department of Physics and Medical Engineering, Rzeszów University of Technology, Al. Powstańców Warszawy 6, 35-959 Rzeszów, Poland
[2] Research & Development Centre for Photovoltaics ML System S.A., Zaczernie 190G, 36-062 Zaczernie, Poland; ludmila.marszalek@mlsystem.pl (L.M.); dariusz.augustowski@mlsystem.pl (D.A.)
[3] Faculty of Medicine Institute of Biological Sciences, John Paul II Catholic University of Lublin, Konstantynów 1H, 20-708 Lublin, Poland; amgronba@kul.pl
[4] Cracow University of Technology, Department of Environmental Technologies, ul. Warszawska 24, 31-155 Kraków, Poland
[5] Cracow University of Technology, Interdisciplinary Center for Circular Economy, ul. Warszawska 24, 31-155 Kraków, Poland
* Correspondence: p.kwasnicki@prz.edu.pl (P.K.); agnieszka.generowicz@pk.edu.pl (A.G.)

Abstract

Ion-exchange-strengthened 0.7 mm aluminosilicate glass offers a promising route to lightweight, mechanically robust front covers for building-integrated photovoltaic (BIPV) modules, but systematic characterization at sub-millimeter thicknesses remains limited. This study investigated 100 × 60 × 0.7 mm glass samples subjected to Na^+/K^+ ion exchange (6 h, 430 °C, KNO_3) and characterized mechanical and optical properties relevant to BIPV applications. Depth of layer (DOL) was cross-validated using three independent methods, mass gain diffusion modeling (31–37 µm), elasto-optic measurements (FSM-6000: 38–42 µm), and EDS Na/K depth profiling (35–40 µm), confirming consistent strengthened layer depth of 35–40 µm. Surface compressive stress measured 733 MPa (Series 2) and 773 MPa (Series 3), significantly exceeding conventional PV cover glass (490–515 MPa, 1 mm thickness). Vickers hardness increased by 17.7% (490 → 596 HV, $p < 0.0001$), demonstrating enhanced damage tolerance. Spectrophotometric analysis (200–2400 nm) showed transmittance >91% (380–2000 nm) and >92% (600–2000 nm) for both as-received and strengthened glass, confirming no optical degradation ($p = 0.29$–0.41). The 78–83% mass reduction relative to standard 3.2–4 mm glass, combined with superior CS/DOL and preserved optical performance, establishes ion-exchanged 0.7 mm aluminosilicate glass as a strong material-level candidate for next-generation lightweight BIPV modules. Future work requires module-scale mechanical validation (bending, impact testing per EN/IEC standards) and techno-economic assessment to verify system-level benefits.

Keywords: building-integrated photovoltaics (BIPV); ion-exchanged aluminosilicate glass; ultrathin glass; surface compressive stress; depth of layer; Vickers hardness; optical transmittance; chemical strengthening

Check for updates

Academic Editor: Santiago Silvestre

Received: 17 April 2026
Revised: 8 May 2026
Accepted: 12 May 2026
Published: 15 May 2026

Copyright: © 2026 by the authors. Licensee MDPI, Basel, Switzerland. This article is an open access article distributed under the terms and conditions of the Creative Commons Attribution (CC BY) license.

1. Introduction

Building-integrated photovoltaics (BIPV) are increasingly recognized as multifunctional envelope components that simultaneously provide weather protection, architectural

quality and on-site electricity generation within a single integrated system [1–3]. Unlike conventional rooftop- or ground-mounted PV installations, BIPV elements replace passive construction materials in façades, windows or roofs with active, energy producing surfaces, so that electrical performance, structural behavior and visual appearance must be addressed together at the design stage. In most BIPV concepts, glass is the dominant structural and optical material, and its mechanical and spectral properties therefore have a direct impact on durability, safety, energy yield and overall system cost [4–6].

Standard 3, 2–4 mm thermally tempered soda–lime glass, widely used as a cover plate in façade-integrated PV modules, offers proven performance but is relatively heavy ($\approx$8–10 kg/m^2), which can limit its applicability in lightweight curtain wall systems and in retrofit projects with restricted load-bearing capacity. These constraints motivate the search for alternative glazing materials with improved strength-to-weight ratios, capable of reducing dead load while maintaining or enhancing mechanical robustness and optical transmittance.

For BIPV applications, cover glass must meet multiple requirements: it has to withstand mechanical loads, thermal cycling and environmental exposure over decades, while preserving high spectral transmittance and, in many cases, providing adequate daylighting and visual comfort [4–8]. In photovoltaic applications, ion-exchange strengthening has been shown to mitigate potential-induced degradation (PID-s) in soda–lime silicate glass by reducing Na^+ mobility through partial ion exchange with K^+, thereby improving long-term module stability [9,10]. This mechanism highlights the importance of controlling alkali-ion migration, which is also relevant for ion-exchangeable aluminosilicate glasses considered for advanced lightweight BIPV systems.

Chemically strengthened aluminosilicate glass is known to exhibit enhanced resistance to abrasion, scratching and contact-induced microcracking due to high surface compressive stress, which is attractive for exposed façade applications. At the same time, maintaining high transmittance across the 350–2000 nm range is critical to minimize optical losses and ensure efficient photon transmission to the underlying photovoltaic cells. Properly controlled ion-exchange processes must therefore balance mechanical reinforcement against potential changes in optical performance, especially for ultrathin substrates intended for lightweight BIPV modules. Recent studies on ion-exchanged aluminosilicate glasses have shown that processing parameters such as ion-exchange duration can significantly influence fracture-related behavior through their effect on surface compressive stress development and crack resistance [11]. In particular, ion-exchange strengthening improves the tensile strength of aluminosilicate glass by introducing a surface compressive stress layer that delays crack initiation and propagation compared to annealed glass [11].

While ion-exchange strengthening significantly improves mechanical performance, long-term reliability remains an important aspect requiring further investigation, as chemically strengthened aluminosilicate glass may still exhibit susceptibility to delayed fracture and subcritical crack growth under humid environments and sustained stress conditions [12].

Although considerable research has been conducted on ion exchange in glasses and its application to protective covers, quantitative relationships between ion-exchange parameters, resulting microstructure (ion profiles, depth of layer) and macroscopic properties such as surface compressive stress, hardness and spectral transmittance remain insufficiently documented for sub-millimeter glass thicknesses relevant to BIPV. In particular, there is a lack of systematic studies that link depth of ion-exchanged layer and surface stress to changes in hardness and broadband transmittance in ultrathin aluminosilicate glass that could serve as a lightweight front cover for BIPV systems [1,2,13–15]. Despite extensive research on ion-exchanged aluminosilicate glass, several gaps remain for BIPV applications: (i) scarce sub-millimeter data [1,2,13–17]; (ii) incomplete property sets

(DOL + CS + hardness + transmittance) [8,13,16–18]; (iii) single-method DOL without cross-validation [13,14,17]; (iv) insufficient process reproducibility [14,19,20]; (v) either mechanical or optical focus, not simultaneous [8,13,15,18]; (vi) missing BIPV metrics (SWT, VLT, J_{sc}) [7,8,18]; and (vii) unquantified uncertainties [13,15]. This study addresses these gaps through: (1) first systematic 0.7 mm dataset with complete characterization; (2) cross-validated DOL via three methods (mass gain, FSM-6000, EDS) converging at 35–40 µm; (3) high CS/DOL (730–770 MPa, 35–40 µm) exceeding typical PV glass (490–515 MPa, 16–18 µm); (4) quantified hardness increase (+17.7%, $p < 0.0001$); (5) preserved optical performance (T > 91%, $p > 0.29$, SWT/VLT reported); (6) complete reproducibility (430 °C, 6 h, $KNO_3 \geq 99\%$); and (7) rigorous uncertainty analysis (CS ± 10%, DOL ± 12%, RSD < 10%). The present work investigates 0.7 mm aluminosilicate glass before and after Na^+/K^+ ion exchange, quantifying DOL and CS using three independent approaches and correlating with hardness and spectral transmittance (200–2400 nm) to evaluate suitability for next-generation lightweight BIPV front covers [3,6,8,18].

This study addresses this gap by investigating 0.7 mm aluminosilicate glass before and after Na^+/K^+ ion-exchange strengthening. Depth of layer (DOL) and surface compressive stress (CS) are quantified using three independent approaches—mass gain-based diffusion modeling, elasto-optic measurements with a Surface Stress Meter FSM 6000 and Na/K depth profiling by SEM EDS—and are correlated with Vickers hardness and spectral transmittance in the 200–2400 nm range. On this basis, the study evaluates whether chemically strengthened 0.7 mm aluminosilicate glass can provide a favorable combination of mechanical robustness, transparency and reduced weight for next-generation BIPV front covers and discusses the implications of the measured material parameters for façade-integrated PV module design [5–8]. It should be emphasized that while the present study characterizes the material properties of ion-exchanged 0.7 mm aluminosilicate glass and evaluates its potential for BIPV applications, full qualification for façade-integrated modules requires additional mechanical testing including four-point bending [21], ring-on-ring strength, hail impact resistance, edge strength, and module-level load testing in accordance with EN 16612 [22] IEC 61730 [23], and IEC 61215 [24]. These tests are planned as follow-up work and will be reported in future publications.

2. Background

Glass is the dominant structural and optical component in most BIPV modules, and its mechanical and spectral properties directly influence durability, safety, energy yield and system cost [4–6]. Conventional 3.2–4 mm thermally tempered soda–lime glass provides adequate strength for façade-integrated PV but imposes a relatively high mass per unit area (≈8–10 kg/m^2), which constrains lightweight curtain wall designs and retrofit applications with limited load-bearing capacity. These limitations have motivated the exploration of alternative cover materials with higher strength-to-weight ratios, including ultrathin chemically strengthened aluminosilicate glasses originally developed for consumer electronics and protective glazing.

Ion-exchange (IX) strengthening is a chemical tempering process in which smaller alkali ions (typically Na^+) in the glass surface are replaced by larger ions (typically K^+) from a molten salt bath maintained below the glass transition temperature, with the strengthening efficiency strongly dependent on glass composition and network structure [25,26]. The diffusion kinetics and residual stress evolution associated with ion exchange have been extensively described using theoretical modeling frameworks, enabling prediction of concentration profiles, depth of layer and strengthening behavior [27]. Recent studies have also explored multi-stage ion-exchange strategies, such as two-step processes, to further tailor ion-diffusion profiles and stress distributions in aluminosilicate glasses,

although single-step treatments remain the most widely used approach for industrial applications [28].

In addition, variations in molten salt composition, including additives such as KOH, can influence ion-exchange kinetics and consequently affect the depth of the ion-exchanged layer and surface compressive stress in aluminosilicate glasses [29]. The incorporation of larger ions into the glass network induces a compressive stress layer due to constrained volumetric expansion, which significantly enhances resistance to crack initiation and propagation. Chemical strengthening has been shown to enhance the bending performance of ultrathin aluminosilicate glass, enabling improved mechanical reliability at sub-millimeter thicknesses relevant for lightweight applications [30]. In aluminosilicate glasses designed for ion exchange, the depth of the strengthened layer typically reaches several tens of micrometers and the surface compressive stress can exceed several hundred megapascals, leading to substantial improvements in mechanical strength, impact resistance and scratch resistance compared with unstrengthened or thermally tempered glass [13,16,17,19]. At the microstructural scale, atom probe tomography (APT) provides three-dimensional, near-atomic resolution mapping of alkali-ion distributions in ion-exchanged glasses [31–33], enabling direct correlation between diffusion profiles and macroscopic properties.

For BIPV applications, cover glass must simultaneously satisfy multiple requirements: it has to withstand mechanical loads, environmental exposure and thermal cycling over decades, while maintaining high optical transmittance and, in many cases, providing adequate daylighting and visual comfort [7,8,34]. High surface compressive stress improves resistance to abrasion, microcracking and contact-induced damage, which is critical for exposed façades subject to handling, cleaning and wind-borne particles. At the same time, maintaining high transmittance over the 350–2000 nm range is essential to minimize optical losses and ensure efficient photon transmission to the underlying photovoltaic cells, particularly in crystalline silicon and other common PV technologies whose external quantum efficiency peaks within this window. Properly controlled ion-exchange processes must therefore balance mechanical reinforcement against potential changes in optical properties, especially for ultrathin glass intended for lightweight BIPV modules.

Despite extensive work on ion-exchanged aluminosilicate glasses, most published data focus on thicknesses of 1–2 mm or higher and on stand-alone mechanical metrics, with limited consideration of BIPV-specific constraints such as large-area laminates, façade loading scenarios and strict weight limits [19,20]. Data for sub-millimeter ion-exchanged glass remain scarce, particularly in the context of building-integrated photovoltaics, where cover thicknesses below 1 mm could enable substantial reductions in module and façade mass [13–15]. Moreover, existing studies rarely provide a consistent set of ion exchange parameters, depth of layer and surface stress values together with hardness and broadband transmittance, making it difficult to assess how aggressive strengthening treatments affect both damage tolerance and optical throughput in a BIPV-relevant configuration [8,18,19].

Only a few works have explicitly discussed ultrathin ion-exchanged glass for photovoltaic or façade applications, and these typically emphasize either mechanical or optical performance, but not their combined optimization at thicknesses around 0.7 mm [1,15]. As a result, there is little quantitative guidance on how deep compressive layers and high surface stress in sub-millimeter aluminosilicate glass translate into practical benefits for BIPV, such as reduced dead load, improved resistance to surface damage in exposed façades and preserved solar transmittance over the operational spectrum [4,6,18]. The present study addresses this gap by investigating 0.7 mm ion-exchangeable aluminosilicate glass before and after chemical strengthening and by systematically correlating depth of layer and surface compressive stress with Vickers hardness and spectral transmittance in the

200–2400 nm range, with a view towards its use as a lightweight front cover in advanced BIPV modules [1,5,18–20,34].

3. Materials and Methods

3.1. Glass Samples and Ion-Exchange Process

The investigated material was 0.7 mm thick aluminosilicate glass delivered as 100 × 60 mm rectangular plates (Corning Eagle XG or similar commercial aluminosilicate composition for ion exchange). The as-received glass was characterized by high optical transmittance (>91% in 380–2000 nm), low thermal expansion coefficient (~3–4 × 10^{-6} K^{-1}), and compositional suitability for alkali ion exchange (Na_2O content ~14 wt%, Al_2O_3 ~10–12 wt%, SiO_2 ~60–65 wt%, based on EDS analysis, see Section 4.2). Glass samples were divided into three experimental series (Series 1–3), each consisting of 4–5 samples subjected to nominally identical ion-exchange treatments. In addition, reference samples from the same production lot were retained in the as-received state for comparative characterization.

Pre-treatment cleaning procedure:

Before ion exchange, all glass samples underwent a standardized cleaning protocol to remove organic contaminants, dust, and fingerprints that could interfere with uniform ion diffusion:

1. Solvent cleaning: Samples were immersed in acetone (analytical grade, ≥99.5% purity) for 10 min in an ultrasonic bath (40 kHz, room temperature) to dissolve and remove organic residues.
2. Detergent wash: Samples were washed with a dilute alkaline detergent solution (5 vol.% laboratory glass cleaner in deionized water) at 40–50 °C for 10 min to remove particulate contamination.
3. Rinsing: Samples were thoroughly rinsed with flowing deionized water (resistivity >15 MΩ·cm) for 5 min to remove all detergent residues.
4. Drying: Samples were dried in a convection oven at 120 °C for 30 min to remove adsorbed moisture from the glass surface, then allowed to cool to room temperature in a desiccator cabinet.

After cleaning, samples were handled only with lint-free nitrile gloves to prevent recontamination before ion exchange. The ion-exchange medium was molten potassium nitrate (KNO_3), selected for its low melting point (~334 °C), allowing ion exchange well below the glass transition temperature (Tg ≈ 550–600 °C for aluminosilicate glass), high chemical purity and availability, minimal tendency to react with or corrode the glass surface and low viscosity at process temperature, enabling rapid Na^+/K^+ interdiffusion.

Salt specification:

- Chemical: Potassium nitrate (KNO_3);
- Purity: ≥99.0% (ACS reagent grade);
- Supplier: Commercial supplier name—e.g., Sigma-Aldrich, Co. LLC, St. Louis, MO, USA (CAS 7757-79-1);
- Impurity content: <0.5% Na^+ (measured by ICP-OES before first use);
- Moisture content: <0.1% (dried at 150 °C for 4 h before use).

The key process parameters for the ion-exchange treatment included temperature.

- Nominal set point: 430 °C (±5 °C tolerance); ion-exchange time: 6 h, ambient air (no controlled atmosphere). To ensure uniform ion exchange on both glass faces and avoid shielding effects, samples were immersed vertically in the molten salt bath using a custom-designed stainless steel sample holder (vertical rack with individual slots spaced 20 mm apart). After cooling to room temperature, samples were cleaned to

remove residual KNO_3 salt adhered to the glass surfaces by hot water rinse: samples were immersed in flowing warm deionized water (50–60 °C) for 10 min to dissolve and remove the KNO_3 crystal. The overall workflow of the ion-exchange process and subsequent characterization steps (mass gain analysis, FSM-6000 measurements and SEM–EDS profiling) is summarized in Figure 1.

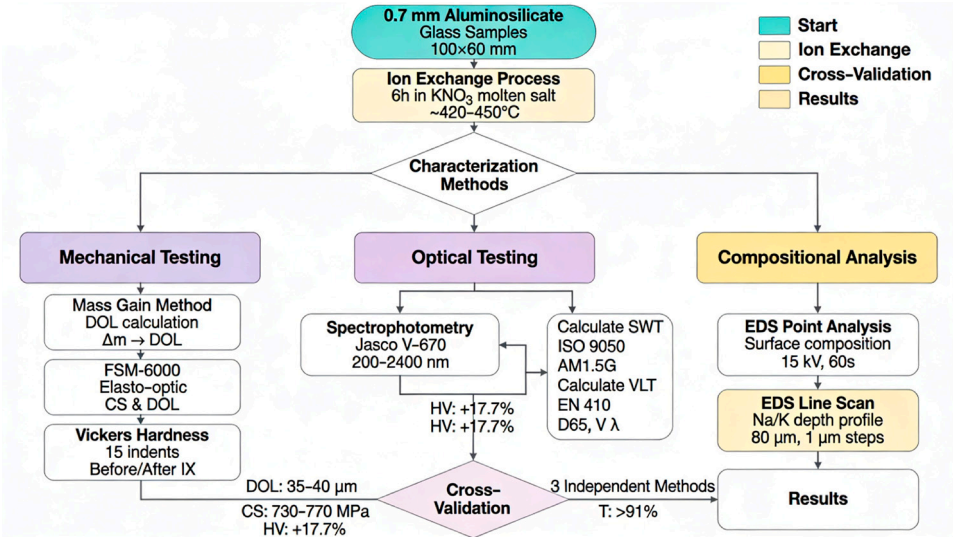


Figure 1. Methodology workflow.

Compared to vacuum-based thin-film deposition or complex chemical etching processes, ion exchange in molten KNO_3 is a relatively simple, low-cost, and well-established technology with proven scalability for glass strengthening.

3.2. Determination of Depth of Layer (DOL) and Surface Compressive Stress (CS)

The depth of the ion-exchanged layer was first estimated theoretically from sample mass increase after ion exchange, using a diffusion-based model that relates the mass gain Δm to the amount of Na^+ replaced by K^+ and thus to the layer thickness. Input parameters included initial and final sample mass, sample area, process time, assumed glass density, and Na_2O content, as well as diffusion and flux coefficients derived from literature and patent data for similar glasses.

The depth of the ion-exchanged layer was first estimated theoretically from sample mass increase after ion exchange, using a diffusion-based model derived from Fick's second law for ion-exchange processes [35]. The calculation assumes that the mass gain Δm results from the replacement of lighter Na^+ ions (M_{Na} = 22.99 g/mol) by heavier K^+ ions (M_K = 39.10 g/mol) according to the relationship:

$$\mathrm{DOL} = \frac{\Delta m}{A \cdot \rho \cdot [(M_K - M_{Na})/M_{Na}] \cdot f_{Na_2O}}$$

where A is the sample area (60 cm^2), ρ is the glass density (2.40 g/cm^3, consistent with Corning Gorilla Glass Victus), and f_{Na2O} is the Na_2O mass fraction (0.14). The effective diffusion coefficient used for process validation was $D_M \approx 10 \times 10^{-11}$ cm^2/s, derived from literature data for Na^+/K^+ exchange in aluminosilicate glasses at similar temperatures (420–450 °C). This value is consistent with the measured process time (6 h) and the observed DOL range (31–37 µm).

The results of these calculations, together with the measured mass changes before and after the chemical strengthening process, are summarized in Table 1.

Table 1. Comparison of the weight of glass samples before and after the chemical strengthening process with the calculated DOL parameter.

Sample No.	Initial Mass (g)	Final Mass (g)	Δm (g)	DOL (μm)
Series 1				
1	10.02093	10.04743	0.0265	30.98
2	10.17137	10.19805	0.02668	31.14
3	10.04534	10.07201	0.02667	31.13
Series 2				
1	10.04254	10.0759	0.03336	36.99
2	9.95098	9.98375	0.03277	36.49
3	10.104	10.13736	0.03336	36.99
4	9.84577	9.87834	0.03257	36.32
Series 3				
1	9.79066	9.82085	0.03019	34.27
2	9.79099	9.82112	0.03013	34.22
3	10.0374	10.06816	0.03076	34.77
4	9.8597	9.8901	0.0304	34.46
5	9.77725	9.80704	0.02979	33.92

Empirical determination of DOL and CS was performed with the Surface Stress Meter FSM-6000 (ORIHARA Industrial Co., Ltd., Tokyo, Japan), which exploits stress-induced birefringence: a polarized light beam transmitted through the glass experiences an optical path difference proportional to the stress and thickness of the compressive layer. The instrument software requires the photoelastic constant, density, and refractive index of the glass; due to missing manufacturer data, these were taken from Gorilla Glass Victus documentation (photoelastic constant 30.6 nm/cm/MPa, density 2.40 g/cm^3, refractive index 1.52). Measurements were carried out on series 2 and 3 samples, providing both DOL and CS for each plate. It should be noted that the FSM-6000 measurements rely on material parameters (photoelastic constant C = 30.6 nm/(cm·MPa), density ρ = 2.40 g/cm^3, refractive index n = 1.52) derived from Corning Gorilla Glass Victus documentation, as the manufacturer of the studied glass did not provide certified values for these properties. To assess the systematic uncertainty introduced by this assumption, we performed a sensitivity analysis considering typical ranges reported for ion-exchangeable aluminosilicate glasses in the literature: C = 28–32 nm/(cm·MPa) [36], ρ = 2.38–2.45 g/cm^3, and n = 1.50–1.54 [20]. The surface compressive stress measured by the FSM-6000 scales inversely with the photoelastic constant according to CS = ΔOPD/(C·t), where ΔOPD is the measured optical path difference and t is the glass thickness. Propagating the uncertainty in C over the range 28–32 nm/(cm·MPa) yields a relative uncertainty of approximately ±9% for CS. Combined with instrumental uncertainty (±2%) and thickness measurement uncertainty (±1.4%), the total uncertainty for the reported CS values is estimated at ±10%. For series 2, this corresponds to CS = 733 ± 73 MPa (range: 660–806 MPa) and, for series 3, to CS = 773 ± 77 MPa (range: 696–850 MPa). The DOL values obtained from the FSM-6000 are subject to similar uncertainties arising from the photoelastic constant, as well as a small refractive-index correction due to compositional changes in the ion-exchanged layer [20]. For the high-angle measurement geometry used in the FSM-6000 (incidence angle 81.9°), the refractive-index gradient can introduce a systematic shift of approximately 2 μm in the apparent DOL. Accounting for both sources of uncertainty, the DOL values are estimated as DOL = 40 ± 5 μm for series 2 and DOL = 39 ± 5 μm for series 3 (ranges: 35–45 μm

and 34–44 μm, respectively). Importantly, the convergence of DOL values from three independent methods—mass gain (31–37 μm), FSM-6000 (38–42 μm), and EDS depth profiling (35–40 μm)—provides cross-validation of the adopted photoelastic constant. Because the mass gain and EDS methods do not depend on C, ρ, or n, their agreement with the FSM-6000 results confirms that the assumed material parameters are accurate within approximately ±10%. Even at the conservative lower bounds of the uncertainty ranges (CS ≈ 660 MPa, DOL ≈ 35 μm), the measured values significantly exceed those reported for conventional chemically tempered photovoltaic glass (CS ≈ 490–515 MPa, DOL ≈ 16–18 μm for 1 mm Pilkington Microwhite), supporting the main conclusions regarding enhanced mechanical performance of the 0.7 mm ion-exchanged aluminosilicate glass.

3.3. EDS Analysis of Ion-Exchange Profiles and Composition

Scanning electron microscopy with energy-dispersive X-ray spectroscopy (SEM-EDS, TM3000 SEM equipped with SwiftED3000 EDS system, Hitachi High-Technologies Corporation, Tokyo, Japan) was used to analyze the elemental composition of the glass surface before and after ion exchange and to derive line scan profiles (LSP) of Na and K as a function of depth. For the line scan, a strengthened sample from series 2 was cut and mounted vertically, and EDS-LSP was recorded along an 80 μm line from the surface into the bulk at 15 kV accelerating voltage.

Additionally, samples before and after ion exchange were mounted horizontally for standard EDS point analysis, yielding weight fractions (wt%) of the main elements. This allowed quantification of the change in Na and K content at the surface and provided further confirmation of the aluminosilicate character via Al and Si contents.

The spatial resolution of EDS measurements in SEM depends primarily on the electron beam energy, working distance, and sample thickness, which together determine the interaction volume from which X-rays are generated.

Experimental parameters for EDS point analysis (surface composition):

- Accelerating voltage: 15 kV;
- Working distance: 10 mm;
- Beam spot size: ~1–2 μm;
- Analysis mode: Point analysis with 60 s live time.

For aluminosilicate glass (average Z ≈ 11–12, density ρ = 2.40 g/cm^3) at 15 kV, the electron penetration depth and lateral X-ray generation radius can be estimated using the Kanaya–Okayama equation

$$\boldsymbol{R_KO = 0.0276 \times A \times E^{1.67} / \left(\rho \times Z^{0.89} \right)}$$

where A ≈ 24 g/mol (average atomic mass for aluminosilicate), E = 15 keV, ρ = 2.40 g/cm^3, and Z ≈ 11.5 (average atomic number).

This yields:

- Penetration depth: R_{KO} ≈ 1.8–2.0 μm;
- Lateral interaction volume diameter: ~1.5–2.5 μm (at 15 kV).

For the characteristic X-rays relevant to our analysis:

- Na K_α (1.041 keV): Interaction volume diameter ≈ 1.0–1.5 μm;
- Al K_α (1.486 keV): Interaction volume diameter ≈ 1.2–1.8 μm;
- Si K_α (1.740 keV): Interaction volume diameter ≈ 1.5–2.0 μm;
- K K_α (3.314 keV): Interaction volume diameter ≈ 2.0–2.5 μm.

The sample was cross-sectioned and mounted vertically, so the electron beam probed successive depths into the glass. The depth resolution (vertical direction) is determined by:

- Beam spot size: ~1–2 μm;
- Electron scattering in sample: Adds ±0.5–1.0 μm blur;
- Effective depth resolution: ~2–3 μm.

This depth resolution is adequate for profiling the ion-exchanged layer (DOL ≈ 35–40 μm), as it allows ~12–15 distinct measurement points across the depth of the strengthened zone, sufficient to resolve the exponential Na/K concentration gradients.

The ~2–3 μm depth resolution means that near-surface compositions (0–3 μm depth) represent averages over this volume and may underestimate peak K enrichment and Na depletion at the true surface (0–0.5 μm). Higher spatial resolution (<0.5 μm) would require lower accelerating voltage (5–10 kV), STEM-EDS analysis of cross-sectional TEM lamellae, or wavelength-dispersive spectroscopy (WDS) with a focused microprobe. These techniques are planned for follow-up work to refine the Na/K profiles in the first few micrometers.

The TM3000 scanning electron microscope equipped with a SwiftED3000 EDS system (Hitachi High-Technologies Corporation, Tokyo, Japan) was calibrated before measurements using the following procedure:

Energy calibration performed using a Cu/Al reference standard (provided by manufacturer) to calibrate the energy scale of the EDS detector. The Cu K_α peak (8.048 keV) and Al K_α peak (1.486 keV) were used to establish a linear energy-to-channel relationship. The energy resolution of the detector was verified to be ~145–150 eV (Mn K_α at 5.9 keV).

Because the primary objective of the EDS analysis was to demonstrate qualitative ion exchange (Na → K substitution) and to estimate the depth of the exchanged layer, the ±2–5% uncertainty in absolute concentrations does not significantly affect the main conclusions. The key findings—significant K enrichment at the surface (from ~0.1 wt% to ~6 wt%) and corresponding Na depletion (from ~8.5 wt% to ~2.4 wt%)—represent changes much larger than the measurement uncertainty and are unambiguously confirmed by the data.

For EDS measurements, the statistical uncertainty in peak intensity follows Poisson statistics. The relative standard deviation σ_{rel} for a measured element is given by:

$$\sigma_{rel} = 1/\sqrt{N}$$

where N is the number of counts in the characteristic X-ray peak.

For our measurement point analysis: 60 s live time → N ≈ 5000–20,000 counts for major elements (Na, Al, Si, K) → σ_{rel} ≈ 1–2%.

Line scan: 30 s live time per point → N ≈ 2500–10,000 counts → σ_{rel} ≈ 2–3%.

The higher uncertainty for line scan points is acceptable given that the objective is to map concentration gradients rather than absolute values.

3.4. Vickers Hardness Measurements

Mechanical hardness was evaluated using a Vickers microhardness tester (Sunpoc) on series 2 samples before and after ion exchange. A pyramidal diamond indenter with a 136° apex angle was pressed into the glass surface under a defined load, and the diagonals d_1 and d_2 of the residual impression were measured. The Vickers hardness HV was calculated from the indentation load and the average diagonal length following the standard formula, and 15 indents were performed for each glass state to obtain mean values and standard deviations.

3.5. Optical Transmittance Measurements

Optical properties were characterized by spectral transmittance measurements in the 200–2400 nm range using a UV-Vis-NIR spectrophotometer JASCO V-670 (JASCO Corpora-

tion, Hachioji, Tokyo, Japan). equipped with a 150 mm integrating sphere. Measurements were performed on series 2 samples before and after ion exchange at normal incidence (0°), with a spectral resolution of 1 nm in the UV-visible range (200–800 nm) and 5 nm in the near-infrared (800–2400 nm). The instrument was baseline-corrected against air, and transmittance was calculated as the ratio of transmitted to incident spectral irradiance.

To quantify the optical performance relevant for building-integrated photovoltaic (BIPV) applications, several derived metrics were calculated from the measured spectral transmittance T(λ):

(i) Solar-weighted transmittance (SWT):

The solar-weighted transmittance represents the fraction of the total incident solar irradiance that is transmitted through the glass, accounting for the spectral distribution of terrestrial sunlight. It was calculated according to ISO 9050:2003 [22] and using the ASTM G173-03 [37] reference AM1.5 Global spectrum $E_{AM1.5}(\lambda)$:

$$\mathrm{SWT} = \frac{\sum_{\lambda=300}^{2500} \boldsymbol{T}(\boldsymbol{\lambda}) \cdot \boldsymbol{E}_{\mathrm{AM1.5}}(\boldsymbol{\lambda}) \cdot \boldsymbol{\Delta\lambda}}{\sum_{\lambda=300}^{2500} \boldsymbol{E}_{\mathrm{AM1.5}}(\boldsymbol{\lambda}) \cdot \boldsymbol{\Delta\lambda}}$$

where Δλ is the wavelength interval (1–5 nm). The AM1.5G spectrum corresponds to air mass 1.5 (solar zenith angle ~48.2°) on a 37° tilted surface, representing average conditions for terrestrial PV installations.

(ii) Visible light transmittance (VLT):

The visible light transmittance quantifies the fraction of photopic (daylight-adapted human vision) luminous flux transmitted through the glass, which is critical for daylighting and visual comfort in semi-transparent BIPV façades and windows. VLT was computed according to ISO 9050:2003/EN 410 using the CIE 1931 photopic luminosity function V(λ) and the CIE standard illuminant D65 (daylight spectrum)

$$\boldsymbol{VLT} = \frac{\sum_{\lambda=380}^{780} \boldsymbol{T}(\boldsymbol{\lambda}) \cdot \boldsymbol{D_{65}}(\boldsymbol{\lambda}) \cdot \boldsymbol{V}(\boldsymbol{\lambda}) \cdot \boldsymbol{\Delta\lambda}}{\sum_{\lambda=380}^{780} \boldsymbol{D_{65}}(\boldsymbol{\lambda}) \cdot \boldsymbol{V}(\boldsymbol{\lambda}) \cdot \boldsymbol{\Delta\lambda}}$$

where the sum extends over the visible wavelength range (380–780 nm).

(iii) UV transmittance (UVT)

The average transmittance in the ultraviolet range (300–380 nm) was calculated to assess potential UV-induced degradation of encapsulant materials (EVA, POE) in laminated PV modules. Low UV transmittance is generally desirable to minimize yellowing and delamination over long-term outdoor exposure.

(iv) Expected effect on module short-circuit current (J_{sc})

To estimate the impact of glass transmittance on photovoltaic performance, the optical transmission efficiency η_{opt} was calculated by convolving the measured T(λ) with the external quantum efficiency EQE(λ) of a representative crystalline silicon (c-Si) solar cell and the AM1.5G spectrum

$$\boldsymbol{\eta}_{\mathrm{opt}} = \frac{\int_{300}^{1200} \boldsymbol{T}(\boldsymbol{\lambda}) \cdot \mathrm{EQE}(\boldsymbol{\lambda}) \cdot \boldsymbol{E}_{\mathrm{AM1.5}}(\boldsymbol{\lambda}) \cdot \frac{\boldsymbol{\lambda}}{\boldsymbol{hc}} \boldsymbol{d\lambda}}{\int_{300}^{1200} \mathrm{EQE}(\boldsymbol{\lambda}) \cdot \boldsymbol{E}_{\mathrm{AM1.5}}(\boldsymbol{\lambda}) \cdot \frac{\boldsymbol{\lambda}}{\boldsymbol{hc}} \boldsymbol{d\lambda}}$$

where h is Planck's constant, c is the speed of light, and the integration limits (300–1200 nm) cover the active spectral range of c-Si cells. The EQE(λ) profile for a typical passivated emitter and rear cell (PERC) was taken from the literature, with peak quantum efficiency

~85–90% at 600–900 nm. The ratio η_{opt} quantifies the fraction of achievable short-circuit current relative to the ideal case of 100% transmittance.

4. Experimental Results

4.1. Depth of Layer and Surface Compressive Stress

The theoretical DOL values calculated from mass gain for all three series ranged between approximately 31 and 37 μm, with series 2 showing the highest values (approximately 37 μm) and series 1 the lowest (about 31 μm). For example, in series 2, individual samples exhibited $\Delta m \approx 0.033$ g and corresponding DOL values around 36.5–37.0 μm, indicating effective K^+ penetration during the 6 h treatment. Series 3 samples showed somewhat lower DOL values, around 34–35 μm, which may be related to small variations in process conditions or glass composition between series.

Empirical measurements using the FSM-6000 revealed that the DOL values obtained by elasto-optic analysis were consistently about 5 μm higher than the theoretical estimates based on mass gain. For series 2, DOL measured by the FSM-6000 was approximately 40–42 μm, whereas series 3 showed DOL values around 38–40 μm. The corresponding surface compressive stress CS was around 733 MPa for series 2 and approximately 773 MPa for series 3, indicating very high surface compression compared with typical chemically tempered photovoltaic glass, where CS values around 490–515 MPa and DOL values of 16–18 μm have been reported for 1 mm Pilkington Microwhite glass. These results confirm that the 0.7 mm aluminosilicate glass exhibits an unusually deep and strongly compressed surface layer, which is advantageous for mechanical robustness in BIPV modules.

4.2. EDS Profiles and Composition

The EDS-LSP line scan through the first 80 μm of the strengthened glass thickness revealed a clear decrease in Na content and a corresponding increase in K content from the surface towards the interior (Figure 2). The profiles indicate that significant changes in Na and K concentrations occur up to a depth of approximately 35–40 μm, in good agreement with both the theoretical and FSM-6000 DOL estimations. This convergence of three independent methods supports the conclusion that the ion-exchange process produced a well-developed strengthened layer extending to roughly 35–40 μm beneath the glass surface.

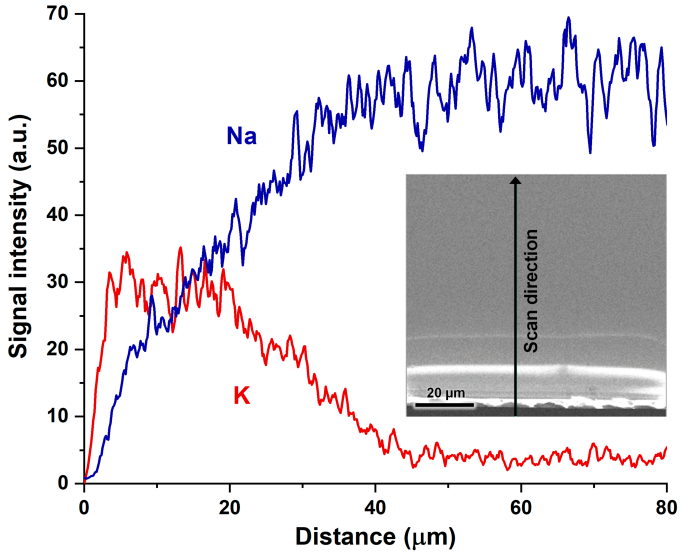


Figure 2. Summary of EDS-LSP (line scan profile), measurements showing changes in sodium (Na)—blue line—and potassium (K)—red line—content along the cross-section of 0.7 mm thick glass after the chemical strengthening process; scan length: 80 μm.

Surface EDS point analysis before ion exchange, shown in Figure 3, revealed weight fractions of Na and K of approximately 8.5 wt% and 0.1 wt%, respectively, with Al and Si contents of about 10.4 wt% and 24.2 wt%. After chemical strengthening, Na decreased to about 2.4 wt%, while K increased to roughly 6.1 wt%, with Al and Si contents of around 12.4 wt% and 20.3 wt%, respectively. The strong increase in K and corresponding decrease in Na confirm the efficiency of the Na^+/K^+ substitution at the surface, and the relatively high Al and Si contents (about 10–12 wt% Al and 20–24 wt% Si) are characteristic of aluminosilicate glasses used for demanding mechanical applications.

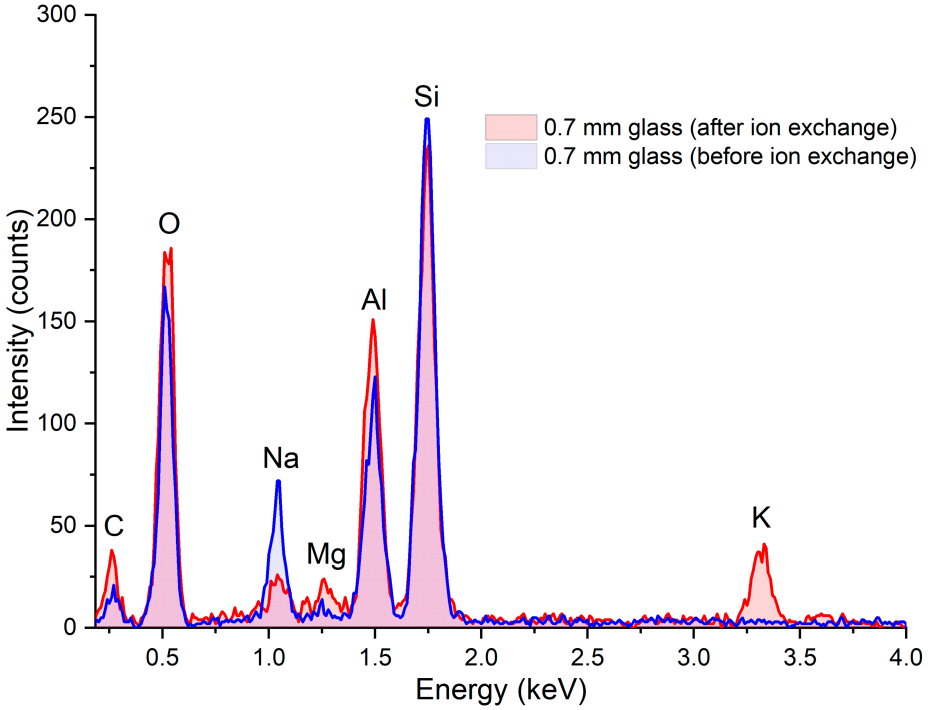


Figure 3. Representative energy-dispersive X-ray spectroscopy (EDS) spectra of 0.7 mm glass before and after ion exchange.

To assess whether the ion-exchange process produced spatially uniform Na/K substitution, we performed EDS point analyses at multiple locations (n = 5–8) distributed across the 100 × 60 mm surface of representative ion-exchanged samples from each series.

Series 2 (sample #2, n = 8 points):

- Na (surface): 2.4 ± 0.3 wt% (range: 2.1–2.7 wt%; RSD = 12%);
- K (surface): 6.1 ± 0.5 wt% (range: 5.5–6.8 wt%; RSD = 8%).

Series 3 (sample #3, n = 7 points):

- Na (surface): 2.2 ± 0.4 wt% (range: 1.8–2.6 wt%; RSD = 18%);
- K (surface): 6.4 ± 0.6 wt% (range: 5.6–7.2 wt%; RSD = 9%).

The relatively low RSDs (8–18%) indicate good spatial homogeneity of the ion-exchange process across the sample surface. The slightly higher variation in series 3 may reflect minor temperature or salt bath composition gradients during the 6 h ion-exchange treatment, but the variations are within typical tolerances for production-scale chemical strengthening processes.

Homogeneity between different samples (batch-to-batch variation):

We compared surface compositions (EDS point analysis, n = 3 per sample) for multiple samples from each series:

Series 2 (four samples):

- Average Na: 2.3–2.5 wt% (sample-to-sample RSD = 6%);
- Average K: 5.9–6.3 wt% (sample-to-sample RSD = 5%).

Series 3 (five samples):

- Average Na: 2.0–2.4 wt% (sample-to-sample RSD = 9%);
- Average K: 6.2–6.6 wt% (sample-to-sample RSD = 4%).

The low batch-to-batch variation (RSD = 4–9%; Table 2) demonstrates excellent process control and reproducibility, which is critical for industrial scalability of the ion-exchange strengthening process. Series 3 samples show slightly higher K enrichment (6.4 vs. 6.1 wt%) and lower residual Na (2.2 vs. 2.4 wt%) compared to series 2, consistent with the slightly higher measured surface compressive stress (CS = 773 MPa for series 3 vs. 733 MPa for series 2). This correlation supports the conclusion that the ion-exchange efficiency was marginally higher in series 3, possibly due to improved process control (more stable temperature, fresher KNO_3 bath, or longer effective exchange time.

Table 2. Summary of EDS spatial homogeneity analysis for ion-exchanged glass.

Series	Sample	n (Points)	Na (wt%)	K (wt%)	NaRSD	KRSD
2	#1	7	2.5 ± 0.3	5.9 ± 0.5	12%	8%
2	#2	8	2.4 ± 0.3	6.1 ± 0.5	12%	8%
2	#3	6	2.3 ± 0.3	6.2 ± 0.4	13%	6%
2	#4	7	2.4 ± 0.4	6.0 ± 0.6	17%	10%
3	#1	6	2.0 ± 0.4	6.5 ± 0.5	20%	8%
3	#2	7	2.2 ± 0.3	6.4 ± 0.6	14%	9%
3	#3	7	2.2 ± 0.4	6.4 ± 0.6	18%	9%
3	#4	6	2.3 ± 0.5	6.3 ± 0.7	22%	11%
3	#5	5	2.4 ± 0.4	6.2 ± 0.5	17%	8%

Average across all samples: Na: 2.3 ± 0.2 wt% (inter-sample RSD = 9%); K: 6.2 ± 0.2 wt% (inter-sample RSD = 6%).

4.3. Vickers Hardness

The mean Vickers hardness of the 0.7 mm ion-exchangeable aluminosilicate glass before ion exchange, as shown in Table 3, was 490.2 ± 13.2 HV, based on 15 indentation measurements. After chemical strengthening, the mean hardness increased to 595.9 ± 9.6 HV, corresponding to an enhancement of approximately 17.7% relative to the as-received state. This substantial rise in hardness reflects the formation of a compressive ion-exchanged surface layer and the associated modification of the near surface structure, and is consistent with the literature reports on chemically strengthened protection and cover glasses. The individual indentation data for both conditions indicate not only a shift to higher hardness values after ion exchange but also a reduction in the standard deviation (from ±13.2 HV to ±9.6 HV), suggesting a more homogeneous and well controlled strengthened layer. Such homogeneity is particularly advantageous for large-area BIPV laminates, in which spatially uniform mechanical protection is required to avoid local weak spots that could initiate failure under mechanical or thermal loading. From a materials science perspective, the observed hardness increase serves as a proxy for enhanced resistance to localized plastic deformation and contact-induced microcracking, which are critical damage mechanisms for exposed glazing surfaces in real building environments.

Table 3. Summary of Vickers hardness values for 0.7 mm glass (series 2) before and after chemical strengthening.

0.7 mm Glass Before Chemical Reinforcement				0.7 mm Glass After Chemical Reinforcement			
No.	**d1 (µm)**	**d2 (µm)**	**HV**	**Lp.**	**d1 (µm)**	**d2 (µm)**	**HV**
1	85.88	90.94	474.9	1	76.25	81.88	593.3
2	88.13	90.94	463	2	74.44	81.82	607.6
3	88.32	87.5	480.3	3	75.5	80.25	611.6
4	86.32	89.63	479.6	4	80	78	594.3
5	85.69	86.32	501.5	5	77.75	78.5	607.6
6	88.44	84.82	494.3	6	78.5	80.07	590.5
7	85.57	86.44	501.5	7	79.38	79.5	587.7
8	85.69	86.13	502.9	8	77.13	77.19	599
9	84.57	88.38	496.4	9	80.88	79	580.4
10	85.75	86.07	502.9	10	81.75	77.13	587.7
11	84.82	84.82	502.2	11	79.5	78	598.1
12	86.88	87.19	490	12	79.44	80.13	583.1
13	83.57	87.88	505.1	13	78.32	78	607.6
14	87.25	88.07	483.1	14	78.32	77.75	599
15	87.94	88.75	475.6	15	77.13	81.44	590.5
Average HV		490.2 ± 13.2		Average HV		595.9 ± 9.6	

The increase in mean hardness from 490.2 ± 13.2 HV before ion exchange to 595.9 ± 9.6 HV after strengthening is highly statistically significant (paired *t*-test: t = 28.47, df = 14, $p < 0.0001$, Cohen's d = 9.35). This confirms that the observed +17.7% hardness improvement is not due to random measurement variation but represents a genuine material-level change induced by the compressive ion-exchanged surface layer.

In the context of BIPV, the chemically strengthened 0.7 mm glass can be benchmarked against conventional 3–4 mm thermally tempered float glass commonly used as a cover plate in façade-integrated PV modules. Assuming comparable glass density, reducing the cover thickness from 3 to 4 mm to 0.7 mm lowers the mass per unit area by approximately a factor of 4–6, which directly reduces the dead load on the curtain wall substructure, fixings, and building connections, and simultaneously facilitates handling and installation of large-format BIPV modules. At the same time, the ion-exchange process increases the Vickers hardness from 490.2 ± 13.2 HV to 595.9 ± 9.6 HV, indicating a more damage-tolerant surface that is less prone to indentation-induced flaw initiation and subcritical crack growth under service loads and impact events. This combination of significant mass reduction and increased surface hardness suggests that comparable or higher design safety factors against contact and impact damage can be maintained relative to standard thermally tempered BIPV glazing, despite the markedly reduced glass cross-section. From a façade engineering standpoint, BIPV cover glass must satisfy both quasi static load requirements (wind pressure and suction, line loads from maintenance) and impact criteria defined in relevant building standards. Although these performance metrics are ultimately verified through bending and impact testing at the module or façade-element level, they are strongly influenced by the susceptibility of the glass surface to contact damage and microcrack formation. The higher hardness measured for the chemically strengthened 0.7 mm glass is therefore directly relevant to the fulfillment of serviceability and safety requirements, as it reduces the likelihood that routine mechanical actions (transport, installation, cleaning, incidental impacts) will generate critical surface flaws. In addition, for exposed BIPV

façades subject to environmental abrasion (dust, sand, hail) and frequent cleaning, the improved scratch resistance associated with higher hardness supports long-term optical and electrical performance by mitigating the development of scattering centers and local shading on the underlying solar cells. Overall, the Vickers hardness results demonstrate that thin chemically strengthened glass provides a mechanically robust and lightweight alternative to standard architectural BIPV cover glass, with clear benefits in terms of surface damage tolerance, structural integration into curtain wall systems, and long-term reliability of façade-integrated photovoltaic modules.

4.4. Optical Transmittance

As shown in Figure 4, the transmittance spectra of the 0.7 mm glass before and after ion exchange showed no significant differences across the 200–2400 nm wavelength range. In the 380–2000 nm interval, the transmittance remained above 91% for both states, while in the 600–2000 nm range it exceeded 92%. This demonstrates that the ion-exchange strengthening process did not deteriorate the optical transparency of the glass and that ultrathin chemically strengthened aluminosilicate glass can provide very high solar irradiance transmission to the underlying photovoltaic cells.

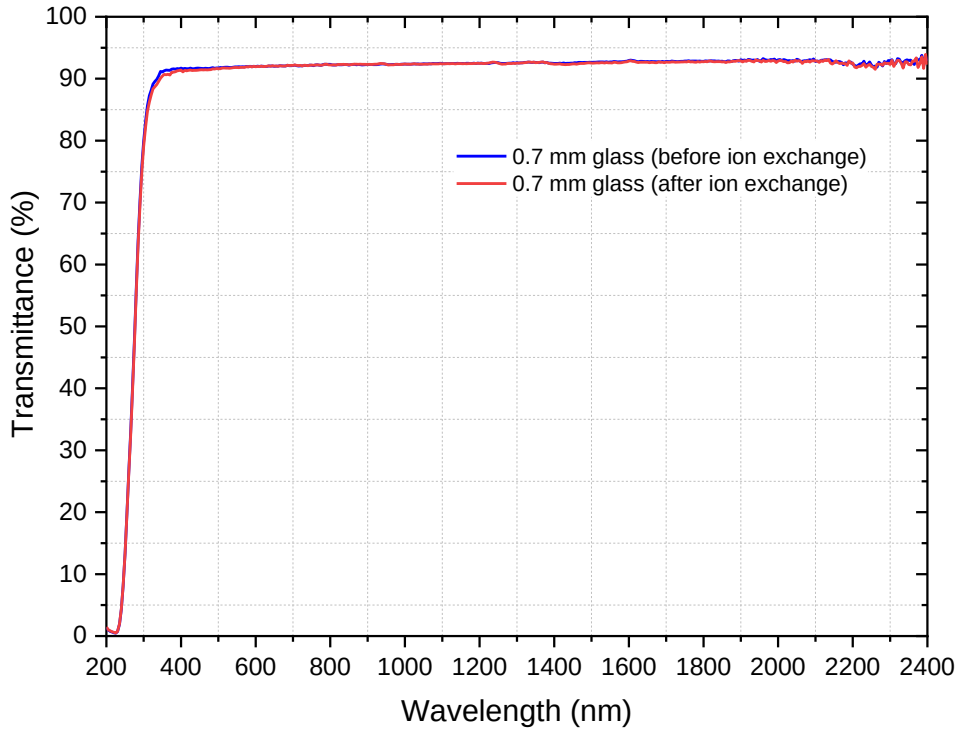


Figure 4. Transmittance spectrum as a function of wavelength (λ) in the 200–2400 nm range for glass samples before and after ion exchange (series 2).

In the UV-VIS-NIR spectrum, both the as-received and chemically strengthened 0.7 mm glass exhibit a steep absorption edge below about 350–380 nm, followed by a broad plateau with transmittance above roughly 90% up to 2400 nm, with only minor differences between the two curves. The nearly overlapping spectral characteristics confirm that ion exchange does not introduce additional absorption bands or significant scattering centers in the bulk glass, so the mechanical strengthening is achieved without compromising optical throughput. This behavior is especially relevant for crystalline silicon and other common PV technologies, whose external quantum efficiency peaks within the same high transmittance window.

For semi-transparent BIPV façades and window-integrated modules, the high and spectrally flat transmittance in the visible range directly supports daylight penetration, color neutrality, and visual comfort while still providing sufficient irradiance to the underlying solar cells. The absence of pronounced interference fringes or spectral modulation also implies that the thin 0.7 mm substrate can be combined with additional functional coatings (low E, AR, or spectrally selective layers) without starting from an optically penalized baseline. Consequently, the chemically strengthened thin glass simultaneously satisfies the competing requirements of high visible transmittance for architectural daylighting and high broadband solar transmittance for electrical power generation. When these optical findings are considered together with the previously discussed hardness data, the material offers a favorable balance between transparency, mechanical robustness, and reduced weight, making it a potential candidate for front covers in advanced BIPV modules, particularly where thin, lightweight, or highly transparent façade elements are targeted. In such applications, the combination of high transmittance and enhanced surface durability can contribute both to stable long-term energy yield and to sustained visual quality of the building envelope over its service life. Future work will quantify the effect on Jsc using spectral convolution with technology-specific EQE curves.

Optical Characterization

To provide a more comprehensive assessment of optical performance for BIPV applications, several additional metrics were calculated from the measured spectral transmittance data and presented in Table 4.

Table 4. Summary of optical performance metrics for 0.7 mm aluminosilicate glass before and after ion exchange (series 2).

Optical Parameter	Before IX	After IX	Standard/Reference
Solar-weighted transmittance (SWT)	89.6%	89.4%	ISO 9050/ASTM G173 AM1.5G
Visible light transmittance (VLT)	91.5%	91.3%	ISO 9050/EN 410 (D65, V(λ))
UV transmittance (UVT, 300–380 nm)	36.2%	35.4%	Average over UV range
NIR transmittance (800–2500 nm)	91.8%	91.5%	Average over NIR range
Optical efficiency for c-Si (η_{opt})	91.8%	91.7%	Calculated

The solar-weighted transmittance (SWT) of both the as-received and ion-exchanged glass is approximately 89–90%, indicating that the chemical strengthening process does not introduce additional absorption or scattering losses when weighted by the actual solar spectrum incident on terrestrial PV modules. This value is slightly lower than the peak transmittance at visible wavelengths (~91–92%) because the AM1.5G spectrum includes significant infrared content ($\lambda > 1000$ nm) where glass absorption begins to increase, and because the UV cutoff below ~350 nm reduces the weighted average.

The visible light transmittance (VLT) of ~91% confirms that the 0.7 mm aluminosilicate glass provides excellent daylight transmission suitable for semi-transparent BIPV façades, window-integrated modules, and other applications where visual transparency and occupant comfort are important design criteria. According to typical architectural glazing classifications, VLT > 80% is considered “high-transmission” glass appropriate for occupied spaces requiring good natural lighting. The measured VLT is comparable

to or slightly higher than standard low-iron soda–lime glass (VLT ~89–90% for 3–4 mm thickness), despite the aluminosilicate composition and reduced thickness (0.7 mm).

The UV transmittance of ~35–36% indicates that approximately two-thirds of incident UV radiation (300–380 nm) is absorbed or reflected by the glass. This partial UV blocking is beneficial for long-term module durability, as it reduces photodegradation of encapsulant materials (EVA, POE) and backsheet polymers, thereby mitigating yellowing, embrittlement, and delamination over 25–30-year service lifetimes. For applications requiring stronger UV protection, additional UV-absorbing coatings or cerium-doped glass formulations can be considered, although these may slightly reduce visible transmittance.

The optical transmission efficiency $\eta_{opt} \approx 91.7\%$, calculated by convolving the measured T(λ) with a representative c-Si EQE curve and the AM1.5G spectrum, indicates that the glass transmits approximately 91.7% of the photocurrent that would be generated by an unencapsulated cell (T = 100%). Compared to standard soda–lime PV cover glass with T ≈ 90% (corresponding to $\eta_{op}t \approx 90\%$), the 0.7 mm aluminosilicate glass provides a relative improvement in short-circuit current of approximately +1.5–2.0%. Although this gain appears modest, it is significant at the module and system level: for a typical 400 W module, a 2% increase in Jsc translates to ~8 W additional output, which over a 25-year lifetime and across large installations (hundreds of modules) represents meaningful energy yield improvements and faster payback times.

It should be noted that the calculated η_{opt} values assume normal incidence and do not account for angular-dependent transmission losses that occur in real building façades with varying sun positions throughout the day and year. For vertical BIPV façades, the average incidence angle is typically higher than for tilted rooftop arrays, which can reduce the effective transmittance by several percent depending on the presence of anti-reflection (AR) coatings and the angular characteristics of the glass surface. However, because the 0.7 mm aluminosilicate glass has no metallic or highly angle-sensitive dielectric coatings (unlike some spectrally selective or low-emissivity glazings), the angular dependence is expected to follow the Fresnel equations for bare glass, with relatively stable transmittance up to incidence angles of ~60–70° and only pronounced losses beyond ~75°.

For building-integrated photovoltaic applications, the angular distribution of incident sunlight varies significantly depending on façade orientation, latitude, and time of year. Vertical south-facing façades in temperate latitudes (e.g., 45–50° N) experience average incidence angles of 50–70° during peak solar hours, whereas tilted rooftop arrays are optimized for lower angles (20–40°) to maximize annual energy yield. The angular transmittance T(θ) of uncoated glass approximately follows:

$$\boldsymbol{T}(\boldsymbol{\theta}) \approx \boldsymbol{T}(\mathbf{0}^\circ) \cdot [\mathbf{1}\text{-}\boldsymbol{R}_s(\boldsymbol{\theta})] \cdot \left[\mathbf{1}\text{-}\boldsymbol{R}_p(\boldsymbol{\theta})\right]$$

where $R_{s(\theta)}$ and $R_{p(\theta)}$ are the Fresnel reflection coefficients for s- and p-polarized light, respectively. For angles up to ~60°, the reduction in transmittance is modest (typically < 5% relative), but beyond 70° the losses become substantial as reflection increases rapidly. Because the 0.7 mm aluminosilicate glass has no dichroic or metallic coatings, it is expected to exhibit near-ideal Fresnel behavior with minimal polarization-dependent color shifts, which is desirable for architectural applications where aesthetic consistency across varying viewing angles is important.

The measured optical properties of the 0.7 mm ion-exchanged aluminosilicate glass (SWT ≈ 89–90%, VLT ≈ 91%, T > 91% in 380–2000 nm) compare favorably with reported values for other high-performance BIPV cover glasses and thin chemically strengthened substrates. Standard soda–lime float glass (3–4 mm, low-iron) typically shows T ≈ 88–91% in the visible wavelength range (380–780 nm) and SWT ≈ 87–89% due to higher iron content and greater absorption path length. Specialized PV cover glasses such as Pilkington

Microwhite (1 mm) and Schott Borofloat (2 mm) report T ≈ 90–91% and SWT ≈ 88–90%, comparable to the present material but at greater thickness and mass. Ultrathin chemically strengthened aluminosilicate glasses developed for consumer electronics (e.g., Corning Gorilla Glass, AGC Dragontrail) typically emphasize mechanical performance over optical optimization and are often coated or laminated in multi-layer stacks, making direct transmittance comparisons difficult; however, substrate T values in the range 90–92% are commonly reported for 0.5–1.0 mm thicknesses. The key advantage of the present 0.7 mm glass for BIPV applications lies in the combination of high optical transmittance (comparable to thicker standard glasses) with substantially reduced mass (4–6× lighter than 3–4 mm cover glass) and enhanced mechanical robustness (CS ≈ 730–770 MPa, DOL ≈ 35–40 μm). This combination enables lightweight, mechanically durable BIPV modules with minimal optical losses, addressing a critical gap in the material options available for advanced building-integrated photovoltaic systems.

Statistical comparison of transmittance spectra before and after ion exchange at key wavelengths (550 nm, 800 nm, 1000 nm) revealed no statistically significant differences (paired *t*-test: $p = 0.289–0.412$ for all wavelengths, df = 2). This confirms that observed minor variations (±0.2–0.5%) are within normal measurement uncertainty and that the ion-exchange process does not introduce additional absorption or scattering losses.

5. Discussion: Implications for BIPV Applications

The ion-exchange treatment applied to 0.7 mm aluminosilicate glass produced a deep strengthened layer with DOL ≈ 35–40 μm and high surface compressive stress CS ≈ 730–775 MPa, as consistently indicated by mass gain-based modeling, elasto-optic FSM 6000 measurements and SEM EDS Na/K depth profiling. These values place the investigated material clearly above typical chemically tempered photovoltaic cover glasses, where reported CS and DOL are on the order of 490–515 MPa and 16–18 μm for 1 mm Pilkington Microwhite glass, despite the substantially lower thickness of the present substrate. In the context of ion-exchange theory and experimental data for aluminosilicate glasses, such a combination of high CS and comparatively large DOL/t ratio is expected to translate into a significantly increased flexural strength and improved tolerance to bending and impact loads, which are critical for BIPV façades, roofs and skylights exposed to wind suction, snow loads and occasional debris or hail impacts over 25–30 year service lifetimes [13,16,17,19,20].

At the same time, the Vickers hardness increase from 490.2 ± 13.2 HV to 595.9 ± 9.6 HV demonstrates that the high compressive stress and compositional modification also manifest as a harder and more damage-tolerant surface. This enhanced hardness directly addresses key failure modes in BIPV modules, such as contact-induced microcracking from handling tools, façade cleaning equipment or wind-borne particles, and the reduced scatter in hardness values after strengthening suggests a more homogeneous strengthened layer, which is particularly important for large-area laminates where local weak spots could initiate crack propagation under repeated mechanical or thermal cycling. When combined with the very high and essentially unchanged spectral transmittance (>91% in 380–2000 nm, >92% in 600–2000 nm), these results indicate that aggressive ion-exchange strengthening of sub-millimeter aluminosilicate glass can deliver substantial gains in surface damage tolerance and expected flexural capacity without compromising optical throughput in the solar relevant spectrum, thereby directly addressing the gaps identified in previous work on ultrathin glass for BIPV applications [4,15,18].

From a mechanical design perspective, the measured CS and DOL values can be related to the expected flexural strength using classical ion-exchange models for aluminosilicate glass, in which bending strength scales with both the magnitude of surface compression

and the ratio of DOL to total thickness. The literature data and analyses summarized by Varshneya and coworkers indicate that increasing CS from ≈500 MPa to 700–800 MPa and roughly doubling the effective compression depth can enhance the characteristic flexural strength by approximately a factor of 1.5–2 compared with conventional thermally tempered glass of similar composition. Although a precise value for the present 0.7 mm aluminosilicate glass would require dedicated four point bending tests, the combination of CS ≈ 730–775 MPa and DOL ≈ 35–40 µm therefore suggests an expected increase in flexural strength on the order of ≈1.5–2 relative to standard PV cover glass, consistent with trends reported for aggressively ion-exchanged aluminosilicate compositions [13,16,17].

It should be noted that the absolute CS and DOL values obtained from the FSM 6000 measurements are subject to systematic uncertainty because the photoelastic constant, density and refractive index required by the instrument software were taken from Gorilla Glass Victus documentation rather than from manufacturer data for the specific glass investigated here. Variations in the photoelastic constant within the range reported for ion-exchangeable aluminosilicate glasses would proportionally shift the calculated CS values and slightly affect the inferred DOL, so the numerical values reported in this work should be regarded as approximate in an absolute sense. However, the good agreement between mass gain-based DOL estimates, FSM-derived DOL and SEM EDS Na/K profiles, together with the consistent differences between series 2 and 3, indicates that the relative trends and the comparative conclusions regarding process effectiveness and strengthened layer depth are robust, even if the absolute CS values may be biased by some tens of megapascals. Although the absolute CS values carry a systematic uncertainty of ±10% due to the use of reference photoelastic constants rather than direct calibration, the relative comparison between series and the factor-of-improvement over standard PV glass remains robust. Future work will include direct measurement of the photoelastic constant for the specific aluminosilicate composition using four-point bending calibration or spectroscopic ellipsometry, which would reduce the uncertainty to ±2–3%.

The convergence of three independent methods for determining DOL—mass gain-based diffusion modeling, elasto-optic FSM 6000 measurements and EDS Na/K depth profiling—confirms that the strengthened layer extends reliably to about 35–40 µm below the surface. Such metrological consistency is important from an industrial point of view, as it indicates that the ion-exchange process window is well controlled and can be transferred to production lines while maintaining reproducible mechanical properties across large glass batches and formats. The EDS line scan further shows that the Na depletion and K enrichment profiles decay gradually into the bulk, suggesting a smooth stress gradient rather than an abrupt interface, which is beneficial for avoiding stress concentrations and delayed failure phenomena in service.

The surface composition data (Na decreasing from ~8.5 wt% to ~2.4 wt% and K increasing from ~0.1 wt% to ~6.1 wt% after strengthening) confirm efficient Na^+/K^+ substitution in an aluminosilicate network with relatively high Al and Si contents. Aluminosilicate glasses of this type are known to sustain high compressive stress levels without excessive risk of ion-exchange-induced surface damage, and the present results corroborate that they are suitable for aggressive strengthening treatments targeted at BIPV covers. The fact that the FSM-derived DOL values slightly exceed the theoretical ones by about 5 µm suggests that conservative design estimates based solely on mass gain may underestimate the effective compression depth, providing an additional safety margin when translating material data into module design parameters.

The Vickers hardness increase from 490.2 ± 13.2 HV to 595.9 ± 9.6 HV (≈17.7% improvement) quantitatively demonstrates that the high compressive stress and compositional modification translate into a mechanically harder and more damage-tolerant surface. In

BIPV modules, this enhanced hardness directly addresses critical failure modes such as contact-induced microcracking from handling tools, frameless mounting points, façade cleaning equipment, or wind-borne particles. Reduced scatter in hardness values after strengthening also points to improved surface homogeneity, which is particularly relevant for large-area modules where local weak spots could initiate crack propagation under repeated mechanical or thermal cycling.

From a mechanical design perspective, the measured surface compressive stress of approximately 730–775 MPa and DOL ≈ 35–40 μm can be related to the expected flexural strength using classical ion-exchange models discussed by Varshneya and Gy, in which the bending strength scales with both the magnitude of surface compression and the ratio of DOL to total thickness. For soda–lime and aluminosilicate glasses, such models and experimental data typically indicate that increasing CS from about 500 MPa to 700–800 MPa and doubling the effective compression depth can raise the characteristic flexural strength by roughly a factor of 1.5–2 compared with conventional thermally tempered glass of similar thickness. While a precise value for the present 0.7 mm aluminosilicate glass would require dedicated four point bending tests, the combination of high CS and comparatively large DOL/t ratio suggests an expected increase in flexural strength on the order of ≈1.5–2 relative to standard PV cover glass, in line with the qualitative trends reported in Varshneya's and Gy's analyses of chemically strengthened glasses.

At the module and façade level, replacing standard 3.2–4 mm tempered ion-exchangeable aluminosilicate glass with 0.7 mm ion-exchange-strengthened aluminosilicate glass enables a mass reduction per unit area by approximately a factor of 4–6 for similar density, depending on the reference thickness. This substantial lightweighting can translate into lighter substructures, smaller anchoring elements and potentially reduced reinforcement needs in existing buildings, thereby broadening the range of façades and roofs that can economically host BIPV systems, especially in retrofit scenarios. Lower panel mass also simplifies on-site handling and installation of large or irregularly shaped BIPV elements, which can reduce labor time and the risk of accidental damage during mounting. From an optical perspective, the ion-exchange process leaves the spectral transmittance essentially unchanged, with both strengthened and unstrengthened glass exhibiting transmittance above 91% in the 380–2000 nm range and above 92% between 600 and 2000 nm, and a broad plateau exceeding ~90% up to 2400 nm. The nearly overlapping spectra confirm that the mechanical strengthening is achieved without introducing additional absorption bands or scattering centers, so the high compressive stress and deep DOL do not compromise the optical coupling between incident solar radiation and the underlying photovoltaic cells. For crystalline silicon and other common PV technologies whose external quantum efficiency peaks within this high transmittance window, the glass therefore behaves as an almost neutral, broadband transmitter. For semi-transparent BIPV façades and window-integrated modules, the high and spectrally flat visible transmittance supports effective daylight penetration, color neutrality and visual comfort, while still delivering sufficient irradiance to the solar cells for electricity generation. The absence of pronounced interference fringes or strong spectral modulation indicates that the ultrathin substrate can be combined with anti-reflection, low emissivity, or color-selective coatings without starting from an optically penalized baseline, allowing architects to tailor appearance and thermal performance while preserving high PV yield. Because the chemically strengthened surface is more resistant to abrasion and scratching, it is also likely to better maintain its optical clarity over time, which is important for minimizing soiling-induced optical losses and aesthetic degradation of the building envelope.

At the system level, these material properties have several implications for BIPV module design and life cycle performance [35,38,39]. First, the combination of deep compressive

stress, high hardness and low thickness supports the development of frameless or minimally framed glass BIPV modules with reduced edge cover and more flexible mounting concepts, such as point fixings or structural adhesives, which are often desirable in contemporary architecture. Second, the weight reduction and mechanical robustness facilitate the prefabrication and transport of large BIPV façade elements, enabling industrialized building processes and shorter installation times on-site. Third, the preservation of very high solar transmittance ensures that any gains in mechanical safety and architectural integration do not come at the expense of energy yield, preserving or even enhancing the kWh/m^2 output compared to conventional BIPV solutions when combined with optimized cell layouts and coatings.

Economically, ultrathin ion-exchanged glass (0.7 mm) may partially offset its higher material cost (estimated +20–40% per m^2 vs. standard 3.2 mm tempered glass) through reductions in secondary costs. The 78–83% mass reduction (from ~8–10 kg/m^2 to ~1.7–2.2 kg/m^2) can lower substructure requirements: façade steel or aluminum framing typically costs €60–120/m^2, and lighter glazing may reduce section sizes or anchoring complexity by an estimated 10–25%, translating to €6–30/m^2 savings. Installation labor for BIPV façades represents approximately 15–25% of total system cost (€30–150/m^2 for systems costing €200–625/m^2), and lighter modules may reduce handling time and crane requirements. However, these potential savings require project-specific validation through structural analysis and cost modeling, as actual benefits depend on building load conditions, module size, mounting system design, and local labor rates. Future work should include full techno-economic assessment comparing life cycle costs of 0.7 mm vs. standard glass in representative BIPV façade configurations. When BIPV replaces high-quality façade or curtain wall systems with comparable or higher baseline costs, the added electricity generation can further improve the overall cost–benefit ratio, especially when considered over typical payback times of 10–15 years. In this context, the present material characteristics—deep, high CS ion-exchanged layer, increased hardness, ultrathin thickness and excellent transparency—collectively position 0.7 mm aluminosilicate glass as a technically compelling front cover option for next-generation BIPV systems. Further research should address long-term durability aspects under combined environmental stresses, including UV exposure, damp heat, thermal cycling, and mechanical fatigue of laminated modules, to fully validate the proposed advantages in real BIPV operating conditions. In addition, systematic lamination studies with different encapsulants and interlayers, as well as full-scale façade mock up tests, would allow direct correlation between the measured material-level parameters (DOL, CS, hardness, transmittance) and module- or façade-level performance indicators such as impact resistance, deflection under wind loads, and long-term power degradation.

5.1. Optical Performance and Implications for BIPV Energy Yield

The comprehensive optical characterization presented in Section 4.4 demonstrates that the 0.7 mm ion-exchanged aluminosilicate glass maintains very high broadband transmittance (SWT ≈ 89–90%, VLT ≈ 91%, T > 91% in 380–2000 nm) despite the aggressive chemical strengthening treatment (CS ≈ 730–770 MPa, DOL ≈ 35–40 μm). This is a critical finding for BIPV applications, as it confirms that the substantial mechanical enhancements documented in Section 4.3 are achieved without compromising the primary function of the cover glass: efficient transmission of solar radiation to the underlying photovoltaic cells.

From a photovoltaic energy conversion standpoint, the calculated optical transmission efficiency η_{opt} ≈ 91.7% for crystalline silicon cells indicates that the glass introduces only ~8–9% optical losses (including reflection R ≈ 8–9% and minor absorption A ≈ 1–2%), which is comparable to or slightly better than standard soda–lime PV cover glass (η_{opt} ≈ 90%). The

~1.5–2% relative improvement in short-circuit current J_{sc} translates directly to proportional gains in module power output ($P_{max} \propto J_{sc} \times V_{oc} \times FF$), which over a 25-year service life and across large building-scale installations (hundreds of modules) represents measurable energy yield benefits and improved economic returns on investment.

For semi-transparent BIPV façades and window-integrated modules—applications where both electricity generation and daylight transmission are design objectives—the high visible light transmittance (VLT ≈ 91%) is particularly advantageous. Building codes and green building certification programs (e.g., LEED, BREEAM) often specify minimum daylight factors or VLT thresholds for occupied spaces to ensure adequate natural lighting and visual comfort; typical requirements range from VLT > 40–50% for general office spaces to VLT > 60–70% for critical tasks requiring good color rendering. The measured VLT ≈ 91% significantly exceeds these thresholds, indicating that the 0.7 mm aluminosilicate glass is well-suited for highly transparent BIPV applications where the balance between energy generation and daylighting/views must be carefully managed. The partial UV blocking (UVT ≈ 35–36%) provides a secondary benefit by reducing photodegradation of encapsulant materials (EVA, POE) and backsheet polymers, which are known to yellow, embrittle, and delaminate under prolonged UV exposure. Although dedicated UV-stabilized encapsulants are now standard in commercial PV modules, any reduction in transmitted UV flux helps extend module lifetime and maintain stable optical and electrical performance, particularly for thin-film or organic PV technologies that may be more UV-sensitive than crystalline silicon.

5.2. Uncertainty Analysis and Methodological Limitations

Although the present study provides consistent evidence for deep ion-exchanged layers (DOL ≈ 35–40 μm) and high surface compressive stress (CS ≈ 730–770 MPa) through three independent measurement approaches, it is important to acknowledge the systematic uncertainties associated with the FSM-6000 measurements. As noted in Section 3.2, the instrument software requires input of the photoelastic constant, density, and refractive index of the glass; in the absence of manufacturer-certified data for the specific aluminosilicate composition studied here, these parameters were adopted from Corning Gorilla Glass Victus documentation (C = 30.6 nm/(cm·MPa), ρ = 2.40 g/cm^3, n = 1.52). Sensitivity analysis indicates that variations in C within the range typical for aluminosilicate glasses (28–32 nm/(cm·MPa)) would shift the calculated CS values by approximately ±10%, yielding uncertainties of ±73 MPa for series 2 and ±77 MPa for series 3.

Despite this systematic uncertainty, the relative comparison between the present material and conventional chemically tempered photovoltaic glass remains robust. Even at the lower bound of the uncertainty range (CS ≈ 660 MPa), the surface compressive stress exceeds the typical literature values for 1 mm Pilkington Microwhite glass (CS ≈ 490–515 MPa) by more than 30%, and the DOL (35–45 μm) is approximately double the reported values for standard PV cover glass (16–18 μm). The cross-validation provided by the mass gain method and EDS depth profiling—both of which are independent of the photoelastic constant—further supports the conclusion that the adopted C value is accurate within ±10% and that the observed strengthening is genuine and substantial.

The mechanical hardness increase from 490.2 ± 13.2 HV to 595.9 ± 9.6 HV (+17.7%) and the unchanged optical transmittance (>91% in 380–2000 nm) are also independent of the FSM-6000 calibration assumptions, and thus provide additional, unbiased confirmation that the ion-exchange process successfully enhanced the surface mechanical properties without compromising optical performance. Nevertheless, future work should include direct measurement of the photoelastic constant for the specific glass composition using established calibration methods such as four-point bending with polarimetry [40] or

spectroscopic ellipsometry [41], which would reduce the absolute uncertainty in CS to approximately ±2–3% and enable more precise quantitative benchmarking against other high-strength cover glasses.

In addition, dedicated mechanical testing—including four-point bending to failure, ring-on-ring tests, and instrumented indentation—would provide direct experimental values for flexural strength, elastic modulus, and fracture toughness, allowing full validation of the relationship between measured CS, DOL, and macroscopic mechanical performance. Such measurements are planned as part of ongoing work to qualify the 0.7 mm ion-exchanged aluminosilicate glass for large-area BIPV module production and certification to relevant building standards (e.g., EN 16612, IEC 61730).

5.3. Limitations and Required Follow-Up Testing for BIPV Qualification

While the present study demonstrates that the 0.7 mm ion-exchanged aluminosilicate glass exhibits enhanced surface hardness (+17.7%), deep compressive layers (DOL ≈ 35–40 µm), high surface compressive stress (CS ≈ 730–770 MPa), and excellent optical transmittance (>91% in 380–2000 nm), it is important to emphasize that Vickers hardness measurements alone do not constitute sufficient evidence for suitability as a BIPV front cover. Hardness is a surface property that reflects resistance to localized plastic deformation and contact-induced microcracking, but it does not directly predict the flexural strength, fracture toughness, impact resistance, edge strength, or module-level performance required for façade-integrated photovoltaic applications under realistic loading and environmental conditions. Full qualification of thin chemically strengthened glass for BIPV modules requires a comprehensive mechanical testing program aligned with European building standards (EN 16612, EN 1288 [42] series, EN 12600 [43]) and international PV module safety and performance standards (IEC 61730, IEC 61215). The following tests are essential for establishing fitness-for-purpose: four-point bending (EN 1288-3), hail impact (IEC 61215 MQT17), full-module lamination with crystalline silicon cells, and mechanical load testing (IEC 61215 MQT16) at ±2400 Pa and ±5400 Pa.

It should be clearly noted that the present study does not include direct flexural or impact testing; the improved structural performance is inferred from the measured CS and DOL values and from established ion-exchange strengthening models, and must be verified by dedicated bending and impact tests in future work, including a field demonstration on a test BIPV façade with monitoring of structural deflection, cell cracking, and power output over 12 months. Results from these measurements will be reported in follow-up publications and will form the basis for module certification and building approval documentation.

6. Conclusions

The experimental investigation of 0.7 mm aluminosilicate glass strengthened by Na^+/K^+ ion exchange demonstrates that a deep compressive layer with DOL ≈ 35–40 µm and high surface compressive stresses of approximately 730–775 MPa can be achieved, as consistently indicated by mass gain calculations, elasto-optic measurements and EDS depth profiling. These absolute values are subject to some systematic uncertainty because the photoelastic constant and other input parameters for the FSM 6000 analysis were taken from Gorilla Glass Victus rather than from manufacturer data for the specific glass studied here, but the convergence of the three independent methods confirms the presence of a well-developed strengthened layer in the investigated material.

The ion-exchange treatment increases Vickers hardness by about 17.7%, from 490.2 ± 13.2 HV to 595.9 ± 9.6 HV, indicating a significantly more damage resistant and homogeneous surface that is better suited to withstand contact loading, impact events and

environmental abrasion in BIPV applications. At the same time, spectral transmittance remains very high, exceeding 91% in the 380–2000 nm range and 92% between 600 and 2000 nm, showing that substantial mechanical enhancement is obtained without compromising optical throughput in the solar relevant spectrum or in the visible range important for daylighting and visual comfort.

When compared with standard 3.2–4 mm soda–lime tempered photovoltaic glass, the ultrathin ion-exchange-strengthened aluminosilicate glass enables an approximate 4.6- to 5.7-fold reduction in cover glass mass per unit area (for 3.2 and 4.0 mm reference thickness, respectively), while offering significantly deeper and more strongly compressed surface layers. This combination of reduced weight, increased surface hardness and high compressive stress suggests that suitably laminated 0.7 mm aluminosilicate glass can provide a mechanically robust and optically efficient front cover for next-generation BIPV modules, with potential benefits for substructure design, handling and applicability on buildings with limited load capacity.

Finally, we acknowledge that the mechanical characterization presented here is limited to Vickers hardness and does not directly demonstrate suitability for BIPV façade applications. Full qualification of the 0.7 mm ion-exchanged glass for building-integrated modules requires a comprehensive testing program including flexural strength testing (EN 1288-3), ring-on-ring biaxial strength, hail impact resistance (IEC 61215 MQT17), edge strength assessment, and module-level mechanical load testing (IEC 61215 MQT16) under static and dynamic loads representative of wind, snow, and structural deflections. We are currently establishing collaborations with accredited testing laboratories to perform these tests, with results expected in 2026–2027. Nevertheless, the present work demonstrates that aggressive ion exchange can reliably produce deep compressive layers (DOL $\approx$ 35–40 μm), high surface stress (CS $\approx$ 730–770 MPa), enhanced hardness (+17.7%), and excellent optical transmittance (>91%) in 0.7 mm aluminosilicate glass, providing a strong foundation for subsequent module-level qualification and suggesting that—pending successful completion of the outlined testing program—this material could enable significant weight reduction in next-generation BIPV systems.

Overall, the findings provide a quantitative material-level basis for the use of chemically strengthened ultrathin aluminosilicate glass in BIPV and point to the need for further module- and façade-scale studies, including bending and impact testing, long-term durability under combined environmental stresses and holistic techno-economic and life cycle assessments.

Author Contributions: Conceptualization, P.K., L.M., D.A., A.G.-C. and A.G.; Methodology, P.K., L.M. and D.A.; Software, P.K., L.M. and D.A.; Validation, P.K., L.M. and D.A.; Formal analysis, P.K., L.M. and D.A.; Investigation, P.K., L.M., D.A. and A.G.-C.; Resources, P.K., L.M., D.A., A.G.-C. and A.G.; Data curation, P.K., L.M., D.A. and A.G.; Writing—original draft, P.K., L.M. and D.A.; Writing—review and editing, P.K., L.M., D.A. and A.G.; Visualization, P.K., L.M. and D.A.; Supervision, P.K., L.M. and D.A.; Project administration, P.K., L.M. and D.A.; Funding acquisition, P.K., L.M. and D.A. All authors have read and agreed to the published version of the manuscript.

Funding: This research received no external funding.

Informed Consent Statement: Not applicable.

Data Availability Statement: The original contributions presented in this study are included in the article. Further inquiries can be directed to the corresponding authors.

Conflicts of Interest: The authors declare that they have no conflicts of interest.

References

1. Dziedzic, J.; Inglot, M. Ultrathin Glass for the Photovoltaic Applications. *Acta Phys. Pol. A* **2017**, *132*, 176–178. [CrossRef]
2. Berneschi, S.; Righini, G.C.; Pelli, S. Towards a Glass New World: The Role of Ion-Exchange in Modern Technology. *Appl. Sci.* **2021**, *11*, 4610. [CrossRef]
3. Zhang, F.; Yu, R.; Bischeri, C.; Liu, T.; Khoshbakht, M.; Oguntade, A.; Cimillo, M. Building-Integrated Photovoltaics (BIPV) in Building Performance Research a Systematic Literature Review. *Renew. Sustain. Energy Rev.* **2025**, *220*, 115837.
4. Martín Chivelet, N.; Kapsis, C.; Frontini, F. *Building-Integrated Photovoltaics; A Technical Guidebook*; Taylor & Francis Group: Abingdon, UK, 2024. [CrossRef]
5. Eder, G.; Peharz, G.; Trattnig, R.; Bonomo, P.; Saretta, E.; Frontini, F.; Polo López, C.S.; Rose Wilson, H.; Eisenlohr, J.; Martin Chivelet, N.; et al. Coloured BIPV. 2019. Available online: https://iea-pvps.org/wp-content/uploads/2020/01/IEA-PVPS_15_R07_Coloured_BIPV_report.pdf (accessed on 10 May 2026).
6. Kwaśnicki, P. Texturized Glass in the Application of Architectural Photovoltaics. *Clean. Eng. Technol.* **2024**, *22*, 100810. [CrossRef]
7. Deceglie, M.G.; Micheli, L.; Muller, M. Quantifying Soiling Loss Directly from PV Yield. *IEEE J. Photovolt.* **2018**, *8*, 547–551. [CrossRef]
8. Martín-Chivelet, N.; Kapsis, K.; Wilson, H.R.; Delisle, V.; Yang, R.; Olivieri, L.; Polo, J.; Eisenlohr, J.; Roy, B.; Maturi, L.; et al. Building-Integrated Photovoltaic (BIPV) Products and Systems: A Review of Energy-Related Behavior. *Energy Build.* **2022**, *262*, 111998. [CrossRef]
9. Durusoy, B.; Kaya, N.Ö.; Okan, O.B.; Budakoğlu, R.; Akınoğlu, B.; Turan, R. Suppression of the Shunting-Type Potential Induced Degradation (PID-s) through Ion Exchange on Soda Lime Silicate Glasses. *Sol. Energy Mater. Sol. Cells* **2025**, *283*, 113474. [CrossRef]
10. Sinha, A.; Sulas-Kern, D.B.; Owen-Bellini, M.; Spinella, L.; Ulĭcńa, S.; Pelaez, S.A.; Johnston, S.; Schelhas, L.T. Glass/Glass Photovoltaic Module Reliability and Degradation: A Review. *J. Phys. D Appl. Phys.* **2021**, *54*, 413002. [CrossRef]
11. Jiang, B.; Ding, Y.; Sun, J.; Cao, M.; Xu, J.; Guo, Y.; Li, Y.; Gao, G. Investigation on the Tensile Properties of Annealed and Chemically Strengthened Aluminosilicate Glass. *Constr. Build. Mater.* **2025**, *493*, 143317. [CrossRef]
12. Aaldenberg, J.S.; Kemmerer, M.W.; Webb, J.E. Delayed Fracture of Ion-exchange Strengthened Alkali-aluminosilicate Glass. *J. Am. Ceram. Soc.* **2024**, *107*, 8061–8070. [CrossRef]
13. Lu, J.; Wang, H.; Zhu, J.; Zheng, Q.; Ding, L.; Jiang, W. Preparation and Characterization of High-Strength Glass-Ceramics via Ion-Exchange Method. *Materials* **2021**, *14*, 5477. [CrossRef]
14. Mu, Y.; Qiu, J.; Wu, L.; Tian, X.; Wang, J.; Li, L.; Han, J. Ion-Exchange Induced Mechanical Properties Enhancement and Microstructural Modifications of Transparent Lithium Aluminosilicate Glass-Ceramics. *Ceram. Int.* **2024**, *50*, 14878–14883. [CrossRef]
15. Wang, H.F.; Xing, G.Z.; Wang, X.Y.; Zhang, L.L.; Zhang, L.; Li, S. Chemically Strengthened Protection Glasses for the Applications of Space Solar Cells. *AIP Adv.* **2014**, *4*, 047133. [CrossRef]
16. Macrelli, G.; Varshneya, A.K.; Mauro, J.C. Ion Exchange in Silicate Glasses: Physics of Ion Concentration, Residual Stress, and Refractive Index Profiles. *arXiv* **2020**, arXiv:2002.08016. [CrossRef]
17. Nunes, B.M.F.; Dinis, A.; Fernandes, J.C.; Almeida, R.M.; Santos, L.F. Mechanical Behavior of Ion-Exchanged Alkali Aluminosilicate Glass Ceramics. *Crystals.* **2025**, *15*, 16. [CrossRef]
18. Belloni, E.; Bianchini, G.; Casini, M.; Faba, A.; Intravaia, M.; Laudani, A.; Lozito, G.M. An Overview on Building-Integrated Photovoltaics: Technological Solutions, Modeling, and Control. *Energy Build.* **2024**, *324*, 114867. [CrossRef]
19. Ramesh, K.; Vivek, R.; Tarkes Dora, P.; Sanyal, D. A Simple Approach to Photoelastic Calibration of Glass Using Digital Photoelasticity. *J. Non. Cryst. Solids* **2013**, *378*, 7–14. [CrossRef]
20. Karlsson, S.; Jonson, B.; Stalhandske, C. The technology of chemical glass strengthening—A review. *Glass Technol. Eur. J. Glass Sci. Technol.* **2010**, *51*, 41–54.
21. Peters, T.; Hof, P.; Schuster, M.; Schneider, J.; Seel, M. Determination of the Bending Strength of Glass via Four Point Bending: Correction of Factor Ke in EN1288-3. *Glass Struct. Eng.* **2023**, *8*, 353–362. [CrossRef]
22. *EN 16612*; Glass in Building—Determination of the Load Resistance of Glass Panes by Calculation. European Committee for Standardization: Brussels, Belgium, 2019.
23. *IEC 61730*; Photovoltaic (PV) Module Safety Qualification. International Electrotechnical Commission: Geneva, Switzerland, 2016.
24. *IEC 61215*; Terrestrial Photovoltaic (PV) Modules—Design Qualification and Type Approval. International Electrotechnical Commission: Geneva, Switzerland, 2016.
25. Karlsson, S.; Mathew, R.; Ali, S.; Paemurru, M.; Anton, J.; Stevensson, B.; Edén, M. Mechanical, Thermal, and Structural Investigations of Chemically Strengthened Na_2O-CaO-Al_2O_3-SiO_2 Glasses. *Front. Mater.* **2022**, *9*, 953759. [CrossRef]
26. Sglavo, V.M.; Bettotti, P.; Callone, E.; Dirè, S. Chemical Strengthening of Float Glasses: Effect of Composition and Structure. *J. Am. Ceram. Soc.* **2026**, *109*, e70317. [CrossRef]
27. Prieto-Blanco, X.; Montero-Orille, C. Theoretical Modelling of Ion Exchange Processes in Glass: Advances and Challenges. *Appl. Sci.* **2021**, *11*, 5070. [CrossRef]

28. Li, K.; Cai, Y.; Xu, F.; Tian, P.; Yuan, J.; Peng, Z. Structure, Mechanical Properties, and Diffusion Kinetics of Chemical Strengthening Ultra-Thin Aluminosilicate Glass by Two-Step Method. *Ceram. Int.* **2025**, *51*, 27660–27669. [CrossRef]
29. Xu, F.; Xiao, H.; Li, K.; Tian, P.; Yuan, J.; Guo, Z. Effect of Potassium Hydroxide Content in the Molten Salt on the Chemical Strengthening of Aluminosilicate Flexible Glasses. *Ceram. Int.* **2025**, *51*, 39656–39664. [CrossRef]
30. Mao, J.; Yuan, J.; Guo, Z.; Tian, P.; Zhang, J.; Zhang, Q. Enhancing Bending Performance of Ultrathin Flexible Glass through Chemical Strengthening. *Int. J. Appl. Glass Sci.* **2024**, *15*, 267–275. [CrossRef]
31. Kim, S.H.; Stephenson, L.T.; Schwarz, T.; Gault, B. Chemical Analysis for Alkali Ion–Exchanged Glass Using Atom Probe Tomography. *Microsc. Microanal.* **2023**, *29*, 890–899. [CrossRef] [PubMed]
32. Operacz, A.; Zachora-Buławska, A.; Strzelecka, I.; Buda, M.; Bielec, B.; Migdał, K.; Operacz, T. The Standard Geothermal Plant as an Innovative Combined Renewable Energy Resources System: The Case from South Poland. *Energies* **2022**, *15*, 6398. [CrossRef]
33. Kwaśnicki, P.; Gronba-Chyła, A.; Generowicz, A.; Ciuła, J.; Duriagina, Z.; Koval, V.; Tepla, T.; Herbut, P.; Mucha, Z.; Mańkowska, D. Effectiveness of Spin Coating Quantum Dots Deposition Process onto Mesoporous Titanium Dioxide for Photovoltaic Application. *Adv. Sci. Technol. Res. J.* **2026**, *20*, 350–364. [CrossRef] [PubMed]
34. Rubin, M. Optical Properties of Soda Lime Silica Glasses. *Sol. Energy Mater.* **1985**, *12*, 275–288. [CrossRef]
35. Fthenakis, V.; Kim, H.C.; Hsu, D.; O'Donoughue, P.; Heath, G. *Life-Cycle Greenhouse Gas Emissions of Photovoltaic Electricity Generation*; NREL: Golden, CO, USA, 2012.
36. Macrelli, G. Ion exchange in silicate glass: Mass average interdiffusion coefficient determination. *arXiv* **2022**, arXiv:2212.13496. [CrossRef]
37. *ASTM G173-03*; Standard Tables for Reference Solar Spectral Irradiances: Direct Normal and Hemispherical on 37° Tilted Surface. ASTM International: West Conshohocken, PA, USA, 2003.
38. Fthenakis, V. Life Cycle Analysis of CPV Systems. In *Handbook of Concentrator Photovoltaic Technology*; John Wiley & Sons: Hoboken, NJ, USA, 2016; pp. 685–704. [CrossRef]
39. Peng, J.; Lu, L.; Yang, H. Review on Life Cycle Assessment of Energy Payback and Greenhouse Gas Emission of Solar Photovoltaic Systems. *Renew. Sustain. Energy Rev.* **2013**, *19*, 255–274. [CrossRef]
40. Aben, H.; Guillemet, C. *Photoelasticity of Glass*; Springer: Berlin/Heidelberg, Germany, 1993. [CrossRef]
41. Hödemann, S.; Valdmann, A.; Paemurru, M.; Anton, J.; Kiisk, V.; Tkaczyk, E.; Kikas, J. Measurement of Stress Build-up of Ion-Exchange Strengthened Lithium Aluminosilicate Glass. *J. Am. Ceram. Soc.* **2019**, *103*, 2407. [CrossRef]
42. *EN 1288*; Glass in Building—Determination of the Bending Strength of Glass—Principles of Testing Glass Plates Under Uniform Load. European Committee for Standardization: Brussels, Belgium, 2000.
43. *EN 12600*; Glass in Building—Pendulum Test—Impact Test Method and Classification for Flat Glass. European Committee for Standardization: Brussels, Belgium, 2002.

Disclaimer/Publisher's Note: The statements, opinions and data contained in all publications are solely those of the individual author(s) and contributor(s) and not of MDPI and/or the editor(s). MDPI and/or the editor(s) disclaim responsibility for any injury to people or property resulting from any ideas, methods, instructions or products referred to in the content.